Unravelling the Intermediate Species of Co_3O_4 Hollow Spheres for CO_2 Photoreduction by In Situ X-ray Absorption Spectroscopy

*Peilei He,[a] Sizhuo Yang,[a] Wenhui Hu,[a] Sungsik Lee,[b] Jier Huang [a]**

[a]Department of Chemistry, Marquette University, Milwaukee, Wisconsin, 53201

[b]X-ray Science Division, Argonne National Laboratory, Argonne, Illinois, 60349

Corresponding Author

*Jier Huang (jier.huang@marquette.edu)

ABSTRACT. Nanostructured hollow materials have emerged as a promising class of materials for energy conversion and storage. In this work, we report a Co_3O_4 hollow sphere nanostructure which can serve as CO_2 reduction catalyst to form CO with high selectivity upon visible light illumination in the presence of $[Ru(bpy)_3]^{2+}$ molecular photosensitizer. Using in situ X-ray absorption spectroscopy, we not only show that Co center in Co_3O_4 hollow sphere is the active site for CO_2 reduction but also identified a key intermediate species, i. e. a reduced Co center due to electron transfer from $[Ru(bpy)_3]^{2+}$ photosensitizer when the system can steadily generate CO.

1. Introduction

Efficient conversion of CO_2 to useful chemical fuels is a promising approach that may sustainably and simultaneously address future energy demand and global warming issues.[1-5] Among the various strategies that have been already developed, photocatalytic CO_2 reduction is perhaps most attractive due to its simplicity and economy of the input energy source.[1, 3, 6-10] As the reduction of CO_2 is an uphill process with high energy barrier, an appropriate photocatalyst is required in order for the reduction reaction to occur at a reasonable rate. As a result, diverse photocatalytic systems for CO_2 reduction have been developed in the past decades.[1-5] One class of these photocatalytic systems that have been intensively studied are the homogeneous photocatalysts based on molecular complexes. However, majority of these homogeneous molecular systems that demonstrate high catalytic efficiency with selectivity are the coordination complexes based on precious metals such as Ru, Re, and Ir,[6-11] where the high cost and scarcity of these metals largely prevent their long term practicality. In addition, these molecular catalysts often suffer from poor photostability during prolonged irradiation as well as the inability for reclylability.[12-15] Due to these reasons, recent focus has geared toward exploring robust heterogenous catalysts mainly based on semiconductors, evidenced by the large number of semiconductor systems evolved in the past decade.[16-21]

Among the various semiconductor photocatalysts that have been reported, nanostructured hollow materials represent one of the most promising photocatalysts for CO_2 reduction due to their inherent advantages over their solid structures.[22-23] For example, the hollow-structured photocatalysts which typically have large specific surface area can facilitate CO_2 adsorption and provide more active sites for the photocatalytic reaction on both the exterior and interior of the shells.[23] In addition, the hollow structure with interior cavity may reduce the distance for charge

transport and enhanced the light absorption due to light scattering and reflection effects in the hollow voids.[24-25] However, the performance of these hollow structure systems for photocatalytic CO_2 reduction in terms of efficiency and selectivity is far from satisfactory.[26-27] Given the distinct benefits to employ hollow structure semiconductors as CO_2 reduction catalysts, such photocatalytic systems are especially ripe targets for further development. Progress in this endeavor will clearly require the fundamental understanding the underlying mechanisms at molecular level.

In this paper, we report a Co_3O_4 hollow sphere CO_2 reduction catalyst, which can effectively reduce CO_2 to form CO with high selectivity (88.6 %) and activity (quantum efficiency of 0.228%) in the presence of $[Ru(bpy)_3]^{2+}$ photosensitizer. Moreover, using in situ X-ray absorption spectroscopy under the standard catalytic conditions, we demonstrated that Co center in Co_3O_4 hollow sphere is the active catalytic site that is responsible for CO_2 reduction and identified a key intermediate species (i.e. reduced Co center) when the photocatalytic reaction reaches equilibrium.

2. Methods

Synthesis of Co-glycolate and Co_3O_4. 0.0582 g of $Co(NO_3)_2$, 6 mL of isopropanol, 6 mL of ethylene glycol, and 0.2 mL of DI water were mixed in a 30 mL Teflon-lined autoclave under 1 h magnetic stirring to give a good mixture. The Teflon-lined autoclave was then heated in an oven at 185°C and maintained at that temperature for 12 hours. After that, the obtained purple powders were collected, washed several times with absolute ethanol, and dried at 60°C for 12 hrs. The Co_3O_4 hollow spheres were obtained by annealing Co-glycolate at 300 ^oC for 2 hrs in air with a ramp rating of 5 ^oC/min.

Photocatalytic CO_2 reduction. $[Ru(bpy)_3]^{2+}$ (bpy = 2,2'-bipyridine) was synthesized

following the published literature procedure.[28] CO_2 photoreduction was performed in 11 mL glass vials with rubber septa. Each sample was made up to a volume of 4 mL, including a certain amount of Co_3O_4 hollow spheres, 1 mg of $[Ru(bpy)_3]^{2+}$, 0.2 mL of TEOA (triethanolamine), as well as CH_3CN and H_2O with different volume ratio. The mixture was purged with CO_2 for 15 min before irradiation by 450 nm LEDs at the optimized power (19 mW). The mixture was kept stirring during photocatalytic reaction. The amount of CO generated was quantified using gas chromatograph by analyzing 200 μL of the headspace.

Characterization. Scanning electron microscopy was performed with a JEOL JSM-6510LV operating in the secondary electron mode. Transmission electron microscopy (TEM) was performed with a JEOL JEM-2100 operating at 200 KV. Powder XRD data were collected by using Rigaku Miniflex II XRD diffractometer with Cu Kα radiation. Steady state and in situ X-ray absorption (XAS) spectra were measured at the beamline 12BM-B at the Advanced Photon

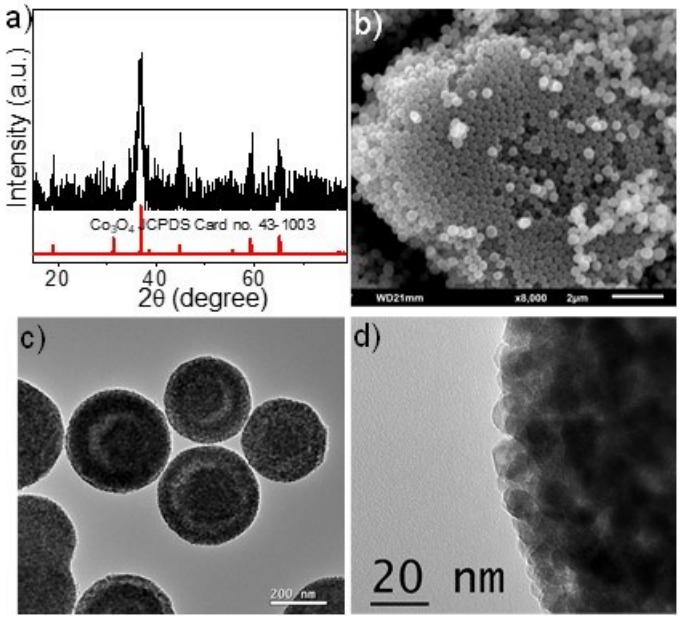

Figure 1. XRD patterns (a), SEM image (b), low-magnification TEM (c), and the magnified TEM images (d) of Co_3O_4 hollow spheres.

Source in Argonne National Laboratory. The conditions for the in situ XAS experiment were 0.5 mg of Co_3O_4, 0.15 mL of TEOA, 0.75 mg of $[Ru(bpy)^3]^{2+}$, 0.57 mL of H_2O, and 2.28 mL of acetonitrile. The amount of CO generated was quantified using Agilent 490 micro gas chromatograph (5 Å molecular sieve column). GC-MS (Agilent Technologies 6850-5973 with HP-PLOT Molesieve column) was used for ^{13}C-label experiment.

3. Results and Discussion

The Co_3O_4 hollow spheres were synthesized by annealing the Co-glycolate sphere at 300 ºC in air for 2 hours. The Co-Glycolate sphere was prepared according to the established synthetic protocols.[29] The X-ray diffraction (XRD) patterns of annealed samples (Figure 1a) agree well with the standard diffraction data of pure Co_3O_4 (JCPDS card No. 43-1003), indicating the formation of Co_3O_4. The SEM image of Co_3O_4 (Figure 1b) shows sphere-like morphology, which resembles that of Co-Glycolate spheres (Figure S1). The low-magnification transmission electron microscopy (TEM) image of Co_3O_4 spheres (Figure 1c) confirmed the hollow structure. The magnified TEM image (Figure 1d) indicates the crystallized phase of the Co_3O_4 hollow spheres which are consisted of small nanocrystals.

In addition to their bulk structure, the local structure of Co_3O_4 nanospheres at Co center was evaluated using steady-state X-ray absorption spectroscopy (XAS). Figure 2a shows the

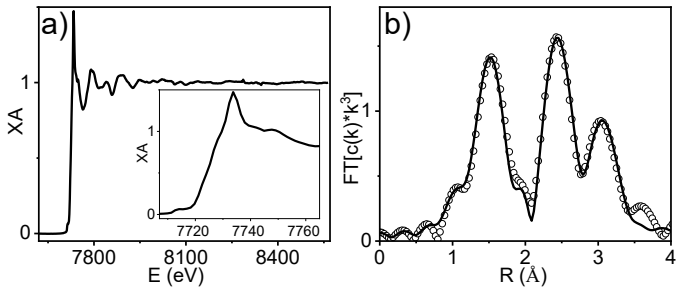

Figure 2. a) X-ray absorption spectrum of Co_3O_4 hollow spheres (solid sample) at Co k-edge. The inset shows the XANES spectrum. b) Fourier-transformed EXAFS spectrum of Co_3O_4 hollow spheres at R-space. The open circles and solid lines are experimental and fitted results, respectively.

extended X-ray absorption fine structure (EXAFS) and X-ray absorption near edge structure (XANES) spectrum (inset) of Co_3O_4 hollow spheres (solid sample) at Co K-edge. The edge energy and the pre-edge feature, consistent with literature results,[30-31] indicate the presence of both T_d Co^{2+} and O_h Co^{3+}, which is expected for spinel structure of Co_3O_4. These results were further supported by the Fourier-transformed EXAFS spectrum in R-space. As shown in Figure 2b, the Fourier-transformed EXAFS spectrum of Co_3O_4 is featured by three peaks, which can be assigned to the convolution of two Co-O bond distance resulting from T_d Co^{2+} and O_h Co^{3+}coordination, Co-Co connected by di-μ-oxo bridge, Co-Co connected by mono--μ-oxo bridge, respectively. The quantitative analysis of these data using FEFF model results in the Co-O distance of 1.93 Å and coordination number 5.33, which is averaged value from two different Co coordination, the four Co-Co distances of 2.86 Å connected by di-μ-oxo bridge, and eight Co-Co distances of 3.36 Å connected by mono--μ-oxo bridge (Table S1). These results are consistent with previous report and further confirm the formation of Co_3O_4 via annealing treatment of Co-glycolate sphere.[30-32]

The catalytic performance of the prepared Co_3O_4 hollow spheres for CO_2 photoreduction was evaluated in the presence of $[Ru(bpy)_3]^{2+}$ (bpy = 2,2'-bipyridine) as photosensitizer and TEOA (triethanolamine) as sacrificial donor under 450 nm LED irradiation. The control experiments that either omit $[Ru(bpy)_3]^{2+}$, TEOA, or Co_3O_4 hollow spheres, or replaces TEOA by TEA (triethylamine) yield negligible amount of CO, suggesting the critical roles of these species play in the CO_2 photoreduction reaction. Previous studies have shown that the amount of water contained in the reaction system has a significant effect on both the activity and selectivity of the catalysts.[33] We thus evaluated the catalytic performance and selectivity of Co_3O_4 hollow spheres for CO_2 reactions by varying the amount of water in the solution. It is interesting to note that,

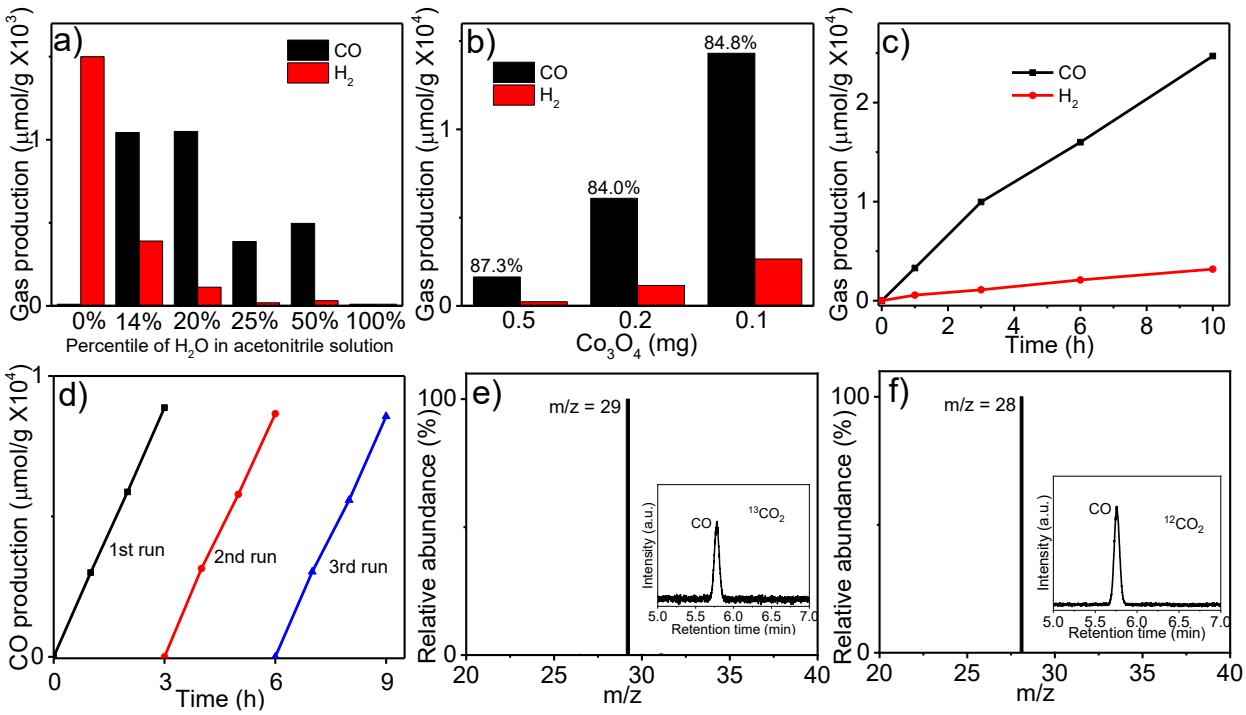

Figure 3. (a) The dependence of CO and H_2 production (μmol/g Co_3O_4) on the amount of H_2O. The reactions were conducted in 1 mg Co_3O_4, 1mg $[Ru(bpy)_3]^{2+}$, and 0.2 mL TEOA. The gas products were collected after 17 hours' illumination; (b) The dependence of CO and H_2 production (μmol/g Co_3O_4) on the amount of catalyst. The reactions were run for 3 hours with 1 mg $[Ru(bpy)_3]^{2+}$, 0.2 mL TEOA, 0.76 mL H_2O, and 3.04 mL acetonitrile; (c) Time profile of CO and H_2 production catalyzed by Co_3O_4 under the optimized conditions (0.1 mg Co_3O_4, 1mg $[Ru(bpy)_3]^{2+}$, 0.2 mL TEOA, 0.76 mL H_2O, 3.04 mL acetonitrile); (d) Recycling of Co_3O_4 catalyst after multiple 3-hour experiments. Mass spectroscopic analyses of the carbon source of the generated CO obtained from the photocatalytic CO_2 reduction reaction under (e) $^{12}CO_2$ and (f) $^{13}CO_2$ (Inset: corresponding gas chromatography of CO). All the photocatalytic reactions were performed under 450 nm (19 mW) light illumination.

without water in the solution (pure acetonitrile), H_2 is the only product (Figure 3a), which suggests that water may not serve as proton source. This is similar to our previous findings, where the system can generate H_2 without water as TEOA can provide protons.[34] Once 0.4 ml of water (14% of the total volume of solvent) was added to the system, more than 1 μmol CO was detected, which results in 72% selectivity for CO formation, suggesting that water is essential for CO_2 reduction to form CO. The enhanced performance for CO_2 reduction upon addition of water might be due to promotion of the reaction kinetics due to reduced thermodynamic barrier in the

presence of water[35] or that the addition of water may induce photolabilization of the bipyridine ligand from $[Ru(bpy)_3]^{2+}$ to form a catalytically active species.[36-37] If the water content was further increased to 20%, the yield of CO remains similar but the selectivity for CO formation increases to 90.5%. Further addition of water results in gradual decrease of the produced CO and H_2 amount until neither CO nor H_2 was produced when the solvent is pure water. These results suggest that both water and acetonitrile are essential for CO production but the presence of large amount of water can inhibit the formation of CO and H_2. One possible reason for the reduced production of CO with water concentration may result from the poor affinity of water to CO_2 molecules.[33] According to these results, the solvent containing 20% of water was used for the following catalytic reactions. Catalytic experiments were also carried out by varying the concentrations of Co_3O_4 hollow spheres. As shown in Figure 3b, the amount of both CO and H_2 decreases with the increasing concentration of the Co_3O_4 hollow spheres, which results in a significant drop of activity in terms of the amount of CO/g of catalyst while the selectivity remains similar. As a result, 0.1 mg of Co_3O_4 hollow spheres were used in the catalytic system for the following experiment.

The full time CO and H_2 generation profiles were measured under the catalytic conditions including 0.1 mg Co_3O_4 hollow spheres, 1 mg $[Ru(bpy)_3]^{2+}$, 0.2 mL TEOA, 0.76 mL H_2O and 3.04 mL acetonitrile. As shown in Figure 3c, under these conditions, the amount of CO and H_2 increase steadily with irradiation time, which can last at least 10 hours, reaching an activity of 24700 μmol/g Co_3O_4 hollow spheres (photon-to-CO efficiency of 0.228 %) and 88.6 % selectivity for CO production. To evaluate the duration of the Co_3O_4 catalytic system, the recycling experiments were explored by collecting Co_3O_4 after each 3 hours' illumination via centrifugation and dispersal in a fresh catalysis solution. As shown in Figure 3d, the system can

be recycled for at least 3 cycles. To validate whether CO was originated from CO_2, we carried out the ^{13}C-labeled isotropic experiment using $^{13}CO_2$ gas under the same catalytic conditions. As shown in Figure 3e, when $^{13}CO_2$ was used as reactant, ^{13}CO (m/z=29) was detected as the product by gas chromatography mass spectrometry, which is distinct from the product of ^{12}CO (m/z = 28) when $^{12}CO_2$ was used (Figure 3f). Furthermore, no other liquid products such as formate or formic acid were detected using NMR and FT-IR (Figure S2). These results confirm that the produced CO originates from photoreduction of CO_2 molecules, not from the decomposition effect of any organics in the system, and that CO is the only product from CO_2 reduction.

To gain mechanistic insight, we measured the in situ XAS spectra of Co_3O_4 catalytic system under the standard catalytic conditions. The in situ XAS spectra at Co k-edge were collected at beamline 12-BM at Advanced Photon Source, Argonne National Laboratory. Figure 4a shows the in situ XANES spectra of Co_3O_4 collected at Co k-edge during the CO_2 photoreduction. These spectra were featured by a prominent absorption in the region of 7720-7730 eV and a small pre-edge feature at ~7715 eV, which can be attributed to the dipole allowed Co 1s-4p transition and dipole forbidden but quadrupole allowed 1s-3d transition. Upon the turn-on of LED lamp, notable changes were observed at the XANES spectra, which can be more clearly seen in the difference XANES spectra (Figure 4b) obtained by subtracting the XANES spectrum before LED illumination from that during LED illumination. Immediately following the illumination (20 mins spectrum), we observed a broad negative feature between 7720-7770 eV, suggesting the decrease of spectral intensity of the in situ XAS spectra. Initially we had thought that this broad negative feature might be an intermediate species at the early stage of CO_2 reduction reaction. However, further in situ XAS experiments under different conditions (e.g.

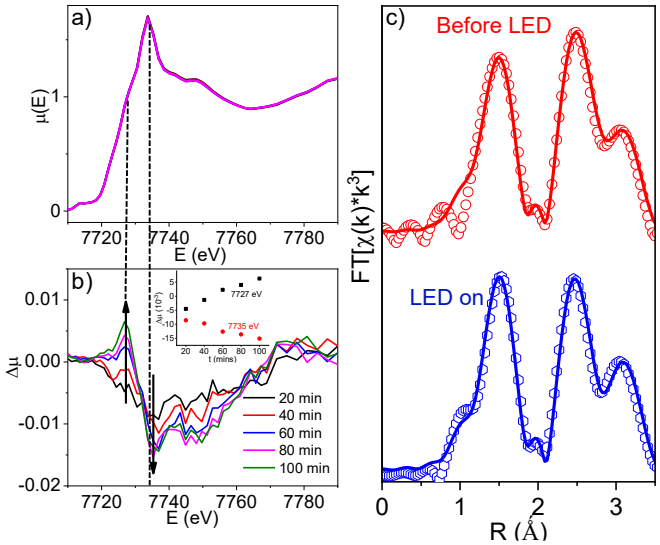

Figure 4. a) The in situ XANES spectra of Co_3O_4 hollow spheres at Co k-edge collected under catalytic conditions (in solution); b) the difference XANES spectrum of Co_3O_4 hollow spheres obtained by subtracting the XANES spectrum collected before LED illumination from those collected during catalysis. The inset plots the intensity of positive feature at 7727 eV and negative feature at 7735 eV as a function of time, which illustrates the evolution of these two features during catalysis. c) The EXAFS spectrum at R-space collected before LED illumination (top panel) and when the system reaches equilibrium during catalysis (bottom panel). The open circles and solid lines are experimental and fitted results, respectively.

excluding LED illumination, $[Ru(bpy)_3]^{2+}$, CO_2, or TEOA etc.) showed that this broad negative signal was always present once XAS measurements initiated (Figure S3), suggesting that this negative feature is not related with light driven CO_2 reduction reaction. While the origin of this spectral feature remains uncertain to us, one possible reason could be that the sample concentration or structure changes slightly due to X-ray illumination. After that, the edge feature gradually grows toward positive signal (7727 eV) while the multi-scattering region (7735 eV) grows further to negative with an isosbestic point (7731.8 eV) between them (Figure 4b and inset), suggesting that these two processes are associated with each other. At about 100 mins after the light irradiation, the XANES spectra stop changing and the positive feature at edge energy is fully developed. These results suggest that the photocatalytic system likely reaches an

equilibrium and the intermediate species under equilibrium is featured by a reduced Co center, which results from the reduction of Co center due to electron transfer from $[Ru(bpy)_3]^{2+}$.

To gain more insight of the intermediate species at equilibrium, we collected the EAXFS spectrum within the time region when the XANES spectra stops changing (~4 hours after light illumination). However, little changes were observed in the EXAFS spectrum at equilibrium compared to the spectrum collected before catalysis (Figure 4c), which is expected due to the small number of surface Co atoms in the hollow spheres. This is further confirmed by quantitative analysis of these EXAFS spectra, where the coordination numbers remain same with slight reduction Co-ligand bond distance due to LED illumination (Table S1 and Figure S4). These results together suggest that the intermediate species at equilibrium undergoes net reduction at Co center without change of nature structure during catalysis.

4. Conclusion

In summary, we report a Co_3O_4 hollow sphere that can efficiently catalyze CO_2 to form CO in the presence of $[Ru(bpy)_3]^{2+}$ as the photosensitizer and TEOA as sacrificial donor under 450 nm LED illumination. Under the optimized conditions, this system can achieve external quantum efficiency of 0.228% with 88.6 % selectivity. More importantly, using in situ X-ray absorption spectroscopy, we identified a key intermediate species that is responsible for CO_2 reduction, i. e. the reduced Co center due to electron transfer from $[Ru(bpy)_3]^{2+}$ to Co_3O_4 hollow sphere. These results not only demonstrated the great potential of Co_3O_4 hollow sphere as photocatalysts for CO_2 reduction but also provided unprecedent new insight on the catalytic mechanism of these hollow materials.

ASSOCIATED CONTENT

Supporting Information. SEM image of Co-glycolate; the fitting parameters of XAS data; difference spectra of in situ XAS measurements under different conditions, and EXAFS spectra in k-space.

AUTHOR INFORMATION

Corresponding Author

*Jier Huang (jier.huang@marquette.edu)

ACKNOWLEDGMENT

This work was supported by National Science Foundation (DMR-1654140) and ACS-PRF (57503-DNI6). Use of the Advanced Photon Source at Argonne National Laboratory was supported by the U. S. Department of Energy, Office of Science, Office of Basic Energy Sciences, under Award No. DE-AC02-06CH11357.

REFERENCES

1. Yu, J.; Low, J.; Xiao, W.; Zhou, P.; Jaroniec, M., Enhanced Photocatalytic Co2-Reduction Activity of Anatase Tio2 by Coexposed {001} and {101} Facets. *J. Am. Chem. Soc.* **2014**, *136*, 8839-8842.
2. Wang, S.; Yao, W.; Lin, J.; Ding, Z.; Wang, X., Cobalt Imidazolate Metal–Organic Frameworks Photosplit Co2 under Mild Reaction Conditions. *Angew. Chem. Int. Ed.* **2014**, *53*, 1034-1038.
3. Kou, Y.; Nabetani, Y.; Masui, D.; Shimada, T.; Takagi, S.; Tachibana, H.; Inoue, H., Direct Detection of Key Reaction Intermediates in Photochemical Co2 Reduction Sensitized by a Rhenium Bipyridine Complex. *J. Am. Chem. Soc.* **2014**, *136*, 6021-6030.
4. Bonin, J.; Robert, M.; Routier, M., Selective and Efficient Photocatalytic Co2 Reduction to Co Using Visible Light and an Iron-Based Homogeneous Catalyst. *J. Am. Chem. Soc.* **2014**, *136*, 16768-16771.
5. Yang, S.; Hu, W.; Zhang, X.; He, P.; Pattengale, B.; Liu, C.; Cendejas, M.; Hermans, I.; Zhang, X.; Zhang, J., et al., 2d Covalent Organic Frameworks as Intrinsic Photocatalysts for Visible Light-Driven Co2 Reduction. *J. Am. Chem. Soc.* **2018**, *140*, 14614-14618.
6. Ishida, H.; Tanaka, K.; Tanaka, T., Photoreduction of Co2 in the [Ru(Bpy)2(Co)2]2+/[Ru(Bpy)3]2+ or [Ru(Phen)3]2+/Triethanolamine/N,N-Dimethylformamide System. *Chem. Lett.* **1987**, *16*, 1035-1038.

7. Gholamkhass, B.; Mametsuka, H.; Koike, K.; Tanabe, T.; Furue, M.; Ishitani, O., Architecture of Supramolecular Metal Complexes for Photocatalytic Co2 Reduction: Ruthenium−Rhenium Bi- and Tetranuclear Complexes. *Inorg. Chem.* **2005**, *44*, 2326-2336.
8. Kumar, B.; Smieja, J. M.; Kubiak, C. P., Photoreduction of Co2 on P-Type Silicon Using Re(Bipy-but)(Co)3cl: Photovoltages Exceeding 600 Mv for the Selective Reduction of Co2 to Co. *J. Phys. Chem. C* **2010**, *114*, 14220-14223.
9. Schneider, J.; Vuong, K. Q.; Calladine, J. A.; Sun, X.-Z.; Whitwood, A. C.; George, M. W.; Perutz, R. N., Photochemistry and Photophysics of a Pd(Ii) Metalloporphyrin: Re(I) Tricarbonyl Bipyridine Molecular Dyad and Its Activity toward the Photoreduction of Co2 to Co. *Inorg. Chem.* **2011**, *50*, 11877-11889.
10. Sato, S.; Morikawa, T.; Kajino, T.; Ishitani, O., A Highly Efficient Mononuclear Iridium Complex Photocatalyst for Co2 Reduction under Visible Light. *Angew. Chem. Int. Ed.* **2013**, *52*, 988-992.
11. Kang, P.; Cheng, C.; Chen, Z.; Schauer, C. K.; Meyer, T. J.; Brookhart, M., Selective Electrocatalytic Reduction of Co2 to Formate by Water-Stable Iridium Dihydride Pincer Complexes. *J. Am. Chem. Soc.* **2012**, *134*, 5500-5503.
12. Tamaki, Y.; Morimoto, T.; Koike, K.; Ishitani, O., Photocatalytic Co₂ Reduction with High Turnover Frequency and Selectivity of Formic Acid Formation Using Ru(Ii) Multinuclear Complexes. *Proc. Natl. Acad. Sci.* **2012**, *109*, 15673-15678.
13. Kobayashi, K.; Kikuchi, T.; Kitagawa, S.; Tanaka, K., Selective Generation of Formamides through Photocatalytic Co2 Reduction Catalyzed by Ruthenium Carbonyl Compounds. *Angew. Chem. Int. Ed.* **2014**, *53*, 11813-11817.
14. Wang, W.; Wang, S.; Ma, X.; Gong, J., Recent Advances in Catalytic Hydrogenation of Carbon Dioxide. *Chem. Soc. Rev.* **2011**, *40*, 3703-3727.
15. McMorn, P.; Hutchings, G. J., Heterogeneous Enantioselective Catalysts: Strategies for the Immobilisation of Homogeneous Catalysts. *Chem. Soc. Rev.* **2004**, *33*, 108-122.
16. Liu, L.; Jiang, Y.; Zhao, H.; Chen, J.; Cheng, J.; Yang, K.; Li, Y., Engineering Coexposed {001} and {101} Facets in Oxygen-Deficient Tio2 Nanocrystals for Enhanced Co2 Photoreduction under Visible Light. *ACS Catal.* **2016**, *6*, 1097-1108.
17. Xu, H.; Ouyang, S.; Li, P.; Kako, T.; Ye, J., High-Active Anatase Tio2 Nanosheets Exposed with 95% {100} Facets toward Efficient H2 Evolution and Co2 Photoreduction. *ACS Appl. Mater. Interfaces* **2013**, *5*, 1348-1354.
18. Gao, S.; Gu, B.; Jiao, X.; Sun, Y.; Zu, X.; Yang, F.; Zhu, W.; Wang, C.; Feng, Z.; Ye, B., et al., Highly Efficient and Exceptionally Durable Co2 Photoreduction to Methanol over Freestanding Defective Single-Unit-Cell Bismuth Vanadate Layers. *J. Am. Chem. Soc.* **2017**, *139*, 3438-3445.
19. Habisreutinger, S. N.; Schmidt-Mende, L.; Stolarczyk, J. K., Photocatalytic Reduction of Co2 on Tio2 and Other Semiconductors. *Angew. Chem. Int. Ed.* **2013**, *52*, 7372-7408.
20. Zhou, M.; Wang, S.; Yang, P.; Huang, C.; Wang, X., Boron Carbon Nitride Semiconductors Decorated with Cds Nanoparticles for Photocatalytic Reduction of Co2. *ACS Catal.* **2018**, *8*, 4928-4936.
21. Fu, Z.-C.; Moore, J. T.; Liang, F.; Fu, W.-F., Highly Efficient Photocatalytic Reduction of Co2 to Co Using Cobalt Oxide-Coated Spherical Mesoporous Silica Particles as Catalysts. *Chem. Commun.* **2019**, *55*, 11523-11526.
22. Zhang, P.; Lou, X. W., Design of Heterostructured Hollow Photocatalysts for Solar-to-Chemical Energy Conversion. *Adv. Mater.*, *0*, 1900281.

23. Xiao, M.; Wang, Z.; Lyu, M.; Luo, B.; Wang, S.; Liu, G.; Cheng, H.-M.; Wang, L., Hollow Nanostructures for Photocatalysis: Advantages and Challenges. *Adv. Mater.*, *0*, 1801369.
24. Wang, X.; Feng, J.; Bai, Y.; Zhang, Q.; Yin, Y., Synthesis, Properties, and Applications of Hollow Micro-/Nanostructures. *Chem. Rev.* **2016**, *116*, 10983-11060.
25. Joo, J. B.; Lee, I.; Dahl, M.; Moon, G. D.; Zaera, F.; Yin, Y., Controllable Synthesis of Mesoporous Tio2 Hollow Shells: Toward an Efficient Photocatalyst. *Adv. Funct. Mater.* **2013**, *23*, 4246-4254.
26. Gao, C.; Meng, Q.; Zhao, K.; Yin, H.; Wang, D.; Guo, J.; Zhao, S.; Chang, L.; He, M.; Li, Q., et al., Co3o4 Hexagonal Platelets with Controllable Facets Enabling Highly Efficient Visible-Light Photocatalytic Reduction of Co2. *Adv. Mater.* **2016**, *28*, 6485-6490.
27. Wang, S.; Guan, B. Y.; Lou, X. W., Rationally Designed Hierarchical N-Doped Carbon@Nico2o4 Double-Shelled Nanoboxes for Enhanced Visible Light Co2 Reduction. *Energy Environ. Sci.* **2018**, *11*, 306-310.
28. Lin, C. T.; Boettcher, W.; Chou, M.; Creutz, C.; Sutin, N., Mechanism of the Quenching of the Emission of Substituted Polypyridineruthenium(Ii) Complexes by Iron(Iii), Chromium(Iii), and Europium(Iii) Ions. *J. Am. Chem. Soc.* **1976**, *98*, 6536-6544.
29. Cheng, M.; Fan, H.; Song, Y.; Cui, Y.; Wang, R., Interconnected Hierarchical Nico2o4 Microspheres as High-Performance Electrode Materials for Supercapacitors. *Dalton Trans.* **2017**, *46*, 9201-9209.
30. Bergmann, A.; Martinez-Moreno, E.; Teschner, D.; Chernev, P.; Gliech, M.; de Araújo, J. F.; Reier, T.; Dau, H.; Strasser, P., Reversible Amorphization and the Catalytically Active State of Crystalline Co3o4 During Oxygen Evolution. *Nat. Commun.* **2015**, *6*, 8625.
31. Fernández-García, M. P.; Gorria, P.; Sevilla, M.; Fuertes, A. B.; Boada, R.; Chaboy, J.; Aquilanti, G.; Blanco, J. A., Co Nanoparticles Inserted into a Porous Carbon Amorphous Matrix: The Role of Cooling Field and Temperature on the Exchange Bias Effect. *Phys. Chem. Chem. Phys.* **2011**, *13*, 927-932.
32. Rosen, J.; Hutchings, G. S.; Jiao, F., Synthesis, Structure, and Photocatalytic Properties of Ordered Mesoporous Metal-Doped Co3o4. *J. Catal.* **2014**, *310*, 2-9.
33. Wang, S.; Wang, X., Photocatalytic Co2 Reduction by Cds Promoted with a Zeolitic Imidazolate Framework. *Appl. Catal. B* **2015**, *162*, 494-500.
34. Pattengale, B.; Yang, S. Z.; Lee, S.; Huang, J., Mechanistic Probes of Zeolitic Imidazolate Framework for Photocatalytic Application. *Acs Catal* **2017**, *7*, 8446-8453.
35. Wang, S.; Hou, Y.; Wang, X., Development of a Stable Mnco2o4 Cocatalyst for Photocatalytic Co2 Reduction with Visible Light. *ACS Appl. Mater. Interfaces* **2015**, *7*, 4327-4335.
36. Ziessel, R.; Hawecker, J.; Lehn, J.-M., Photogeneration of Carbon Monoxide and of Hydrogen Via Simultaneous Photochemical Reduction of Carbon Dioxide and Water by Visible-Light Irradiation of Organic Solutions Containing Tris(2,2′-Bipyridine)Ruthenium(Ii) and Cobalt(Ii) Species as Homogeneous Catalysts. *Helv. Chim. Acta* **1986**, *69*, 1065-1084.
37. Lehn, J.-M.; Ziessel, R., Photochemical Reduction of Carbon Dioxide to Formate Catalyzed by 2,2ť-Bipyridine- or 1,10-Phenanthroline-Ruthenium(Ii) Complexes. *J. Organomet. Chem.* **1990**, *382*, 157-173.

TOC Graphic

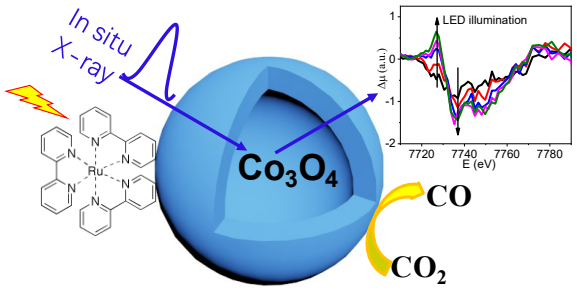
In situ
X-ray
Co3O4
CO
CO2
LED illumination
Δμ (a.u.)
E (eV)
7720
7740
7760
7780
1
0
-1
-2